8-21-2011

Investigation of dose perturbations and the radiographic visibility of potential fiducials for proton radiation therapy of the prostate

Jessie Y. Huang
University of Texas Graduate School of Biomedical Sciences at Houston

Wayne D. Newhauser
University of Texas Graduate School of Biomedical Sciences at Houston

X. Ronald Zhu
University of Texas Health Science Center at Houston

Andrew K. Lee
University of Texas Health Science Center at Houston

Rajat J. Kudchadker
University of Texas Graduate School of Biomedical Sciences at Houston

Recommended Citation

Huang, J., Newhauser, W., Zhu, X., Lee, A., & Kudchadker, R. (2011). Investigation of dose perturbations and the radiographic visibility of potential fiducials for proton radiation therapy of the prostate. *Physics in Medicine and Biology, 56* (16), 5287-5302. https://doi.org/10.1088/0031-9155/56/16/014

Published in final edited form as:
Phys Med Biol. 2011 August 21; 56(16): 5287–5302. doi:10.1088/0031-9155/56/16/014.

Investigation of dose perturbations and radiographic visibility of potential fiducials for proton radiation therapy of the prostate

Jessie Y. Huang[1,2], **Wayne D. Newhauser**[1,3], **X. Ronald Zhu**[3], **Andrew K. Lee**[4], and **Rajat J. Kudchadker**[1,3]

[1]The University of Texas at Houston Graduate School of Biomedical Sciences, 6767 Bertner Avenue, S3.8344, Houston, TX 77030, USA

[2]Department of Imaging Physics, The University of Texas MD Anderson Cancer Center, 1515 Holcombe Boulevard, Unit 193, Houston, TX 77030, USA

[3]Department of Radiation Physics, The University of Texas MD Anderson Cancer Center, 1515 Holcombe Boulevard, Unit 94, Houston, TX 77030, USA

[4]Department of Radiation Oncology, The University of Texas MD Anderson Cancer Center, 1515 Holcombe Boulevard, Houston, TX 77030, USA

Abstract

Image guidance using implanted fiducial markers is commonly used to ensure accurate and reproducible target positioning in radiation therapy for prostate cancer. The ideal fiducial marker is clearly visible in kV imaging, does not perturb the therapeutic dose in the target volume, and does not cause any artifacts on the CT images used for treatment planning. As yet, ideal markers that fully meet all three of these criteria have not been reported. In this study, twelve fiducial markers were evaluated for their potential clinical utility in proton radiation therapy for prostate cancer. In order to identify the good candidates, each fiducial was imaged using a CT scanner as well as a kV imaging system. Additionally, the dose perturbation caused by each fiducial was quantified using radiochromic film and a clinical proton beam. Based on the results, three fiducials were identified as good candidates for use in proton radiotherapy of prostate cancer.

Keywords

proton therapy; fiducial markers; dose perturbation; prostate cancer

1. Introduction

Advances in radiation therapy have led to an increase in the conformality of modern treatments. With increasingly conformal treatment options, such as 3-D conformal radiotherapy (3D-CRT), intensity modulated radiotherapy (IMRT), and proton therapy, dose escalation is possible while simultaneously decreasing margins around the target volume and thus reducing normal tissue toxicities. For prostate therapy, increased dose to the tumor is associated with better outcomes (Fuller and Scarbrough, 2006). However, decreased margins necessitate more accurate and reproducible patient positioning and target alignment. For prostate radiation therapy, target alignment is complicated by internal movement of the prostate within the pelvis (Nederveen *et al*., 2003) caused by variations in bladder and rectal

Corresponding Author: Rajat J. Kudchadker, The University of Texas M D Anderson Cancer Center, 1220 Holcombe Boulevard, Unit 1202, Houston, TX 77030, USA, Phone: 713-563-2538, Fax: 713-563-6949, rkudchad@mdanderson.org.

filling (Kupelian *et al*., 2005). Several strategies have been employed to overcome these positioning problems, including use of rectal balloons, daily CT scans, urethral catheters, transabdominal ultrasonography, and image-guided radiotherapy (IGRT) using implanted fiducial markers (Welsh *et al*., 2004). Serago *et al*., (2006) showed that target positioning with the use of kilovoltage (kV) imaging of fiducial markers was more consistent with electronic portal imaging (EPI) than positioning based on ultrasound, the most common alternate method to implanted fiducial markers for prostate positioning. IGRT with fiducial markers has recently become the state of the art in external beam prostate radiotherapy. In fiducial marker-based IGRT, daily radiographic images reveal the position of the markers, enabling precise alignment of the target with the treatment beam (Hsu *et al*., 2007). However, a disadvantage of this technique is that implanted fiducial markers perturb the radiation beam and cause downstream dose shadows in both a photon beam (Chow and Grigorov, 2005) and a proton beam (Newhauser *et al*., 2007a; Newhauser *et al*., 2007b; Ptaszkiewicz *et al*., 2010; Giebeler *et al*., 2009). Furthermore, fiducial markers made of high-Z (atomic number) materials, such as gold, can also cause significant streak artifacts on computed tomography (CT) images that are used for treatment planning. These potential drawbacks must be taken into account when choosing a fiducial marker for prostate therapy and weighed against the benefits of superior target positioning. For proton therapy of prostate cancer, the ideal fiducial marker is visible in kV images used for daily alignment, causes no dose perturbations in a proton beam, and causes no streak or void artifacts on CT images (Cheung *et al*., 2010). Ideal fiducial markers that meet all three of these criteria do not currently exist. However, many candidate markers are available for evaluation to determine if they are clinically acceptable, if not perfect in all respects. In this study, a total of twelve fiducial markers of different shapes, sizes, and material compositions were evaluated along these criteria as potential candidates for use in proton radiation therapy of the prostate.

2. Methods and Materials

2.1 Fiducials

One of the twelve fiducial markers is a barbell-shaped fiducial (Carbon Medical Technologies, Inc, St. Paul, Minnesota) composed of a proprietary ZrO_2 core coated with a outer layer of carbon (BiomarC®), which is currently in clinical use at The University of Texas M. D. Anderson Cancer Center for prostate localization in patients receiving proton therapy**.** The remaining eleven fiducials are prototype fiducials (Carbon Medical Technologies, Inc) with shapes, material compositions, and dimensions listed in Table 1. The dimensions and mass of each fiducial were measured and crosschecked against specifications from the manufacturer and were used to estimate the average density of each fiducial.

2.2 Radiographic visibility

The radiographic visibility of the fiducials was assessed by acquiring CT images and kV radiographic images of the fiducials in a pelvic anthropomorphic phantom (RANDO®, The Phantom Laboratory, Salem, NY). The section of the phantom that was imaged was approximately 27 cm in the AP direction and 40 cm in the lateral direction. The fiducials were placed inside plastic tubes that fit snuggly into specially drilled holes in the phantom and were backfilled with tissue-equivalent bolus material in order to avoid artifacts caused by air gaps. CT images of the phantom were acquired using a 16-slice scanner (GE Healthcare, Waukesha, WI) with a pelvis scanning protocol (120 kVp, 250 mAs, 2.5 mm slice thickness, 1.27 mm pixel spacing). kV images were acquired using a kV on-board imaging (OBI) system on an electron linear accelerator (Clinac 21EX linear accelerator, Varian Medical, Palo Alto, CA) at our institution with the following techniques:120 kVp,

200 mA, and 630 ms for lateral images and 75 kVp, 200 mA, and 80 ms for AP images. For each kV image, a single fiducial was inserted into the phantom at the approximate location of the prostate in order to closely mimic a patient with an implanted fiducial marker. Setup images of patients are typically acquired in orthogonal pairs just prior to treatment. Thus in our study, we imaged the phantom using kV x-rays at orthogonal cardinal angles (0 degrees and 90 degrees or 0 degrees and 270 degrees).

2.3 Quantification of CT streak artifacts

The artifacts caused by each fiducial were quantified by analyzing the CT images of the fiducials inside the pelvic phantom. For each fiducial, a ring-shaped region of interest (ROI) was defined; this ROI was centered at the position of the fiducial and included the area between an inner radius of 4 pixels and an outer radius of 10 pixels. This ROI was chosen to include the streak artifacts that emanate radially outward from the fiducial and to exclude fiducial itself. A streak index for quantifying the streak artifacts was defined as $SI = \frac{|HU_{\max} - HU_{\min}|_{\text{artifact}}}{\sigma(HU)_{\text{true}}}$, where HU_{max} and HU_{min} are the maximum and minimum CT numbers inside the ROI and $\sigma(HU)_{true}$ is the standard deviation of the CT numbers in 20 pixels in a homogenous region of the phantom that was free of any streak artifact. *SI* is a metric used for quantifying the severity of streak artifacts and is similar to the index employed by Imai *et al* (2009).

2.4 Dose Perturbation Measurements

2.4.1 Proton Beam—In order to quantify the dose shadows caused by each fiducial in a proton beam, measurements were performed using the commercial treatment system (Probeat; Hitachi Ltd., Tokyo, Japan) at our institution (Newhauser *et al*., 2007b). The treatment setup was chosen to closely mimic an actual prostate treatment. For these measurements, we used a 225 MeV passively-scattered proton beam with a range in water of 26.9 cm and a spread out Bragg peak (SOBP) of 10 cm. The system used was a fixed-beam system with a small size snout, which contained a 10 cm × 10 cm final collimating aperture made of brass.

2.4.2 Radiochromic Film—Proton absorbed dose was measured using radiochromic film (Gafchromic EBT2, lots F04090903 and F08130902A; International Specialty Products, Wayne, NJ). The films were digitized using a flatbed scanner (Expression 10000XL, Epson, Long Beach, CA) in landscape orientation into 48-bit color images at a spatial resolution of 72 dpi. The films were scanned prior to irradiation in order to obtain the background optical density and then scanned approximately 72 hours following irradiation. In order to convert net optical density to absorbed dose, a calibration curve was created by irradiating film at a water-equivalent depth of 21 cm to absorbed doses ranging from 1 Gy to 6 Gy. A separate calibration curve was prepared for each lot of film. The suitability of radiochromic film for proton beam dose measurements has been previously documented (Daftari *et al*., 1999; Vatnitsky, 1997; Niroomand-Rad *et al*., 1998; Piermattei *et al*., 2000; Butson *et al*., 2003; Soares, 2006).

2.4.3 Phantom Setup and Irradiation—In order to measure the maximum dose perturbation caused by each fiducial, a small ($12 \times 6 \times 3.5$ cm^3) polymethyl methacrylate (PMMA) phantom was used; the phantom consists of a stack of 1 mm slabs of PMMA mounted together with nylon nuts and screws to form a block. The fiducials and radiochromic films were sandwiched between the PMMA slabs. The phantom was mechanically compressed to minimize air gaps. The twelve fiducials were split into two batches of six fiducials each. For each batch, the fiducials were implanted in a polystyrene foam board and oriented with the long axis of the fiducial perpendicular to the direction of

the beam; the entire board was then sandwiched into the PMMA phantom. Measurements were taken with the fiducials located at water-equivalent depths in the phantom of 22.2 cm (approximately middle of the SOBP) and 25.7 cm (near the end of range of the proton beam). For each fiducial implantation depth, radiochromic films were placed distal to the fiducials in 1 mm increments (1.157 mm water equivalent thickness (WET)) in order to study the effects of dose perturbation as a function of distance downstream from the fiducial; twelve films were used for each fiducial implantation depth. Only three films were sandwiched into the phantom for each irradiation in order to minimize the range shift caused by the film.

2.4.4 Radiochromic Film Analysis of Dose Perturbations—The digitized images of the radiochromic films were analyzed using public domain image processing software (ImageJ, National Institute of Health, Bethesda, MD). In order to quantify the dose perturbation caused by the presence of a particular fiducial, optical transmission values at the location of the fiducial were compared to a reference transmission value, which was obtained from an unperturbed region of the same film. Transmission values were averaged over different areas depending on the size of the fiducial under study: 3×3 pixels (1.06 ×1.06 mm^2) for spherical fiducials, 5×3 pixels (1.76 ×1.06 mm^2) for ZrO_2/Pebax® polymer fiducials, 5×5 pixels (1.76 ×1.76 mm^2) for unperturbed reference and background measurements, and 5×2 pixels (1.76 ×0.71 mm^2) for all other fiducials. Sample pieces of film are shown in Figure 1 to illustrate this process. These average transmission values were then used to calculate the net optical density and relative proton absorbed dose.

2.4.5 Physical Analysis of Dose Perturbations—In order to better understand why certain fiducials cause greater dose perturbations when placed in the path of a clinical proton beam, we tested for correlations between dose and proton linear stopping power and scattering power. The proton linear stopping power $\frac{dE}{dx}$ is proportional to $\frac{\rho Z}{A}$. Therefore, the amount of energy dE lost by a proton when it travels through a fiducial is approximately proportional to $\frac{\rho t Z}{A}$, where ρt is the mass thickness of the fiducial along the direction of the beam. The change in the characteristic scattering angle per path length traveled $\frac{d\theta_{RMS}}{dx}$ is proportional to $Z\sqrt{\frac{\rho}{Ax}}$ (Newhauser *et al*., 2007b). Therefore, the change in characteristic scattering angle caused by a particular fiducial $d\theta_{RMS}$ is approximately proportional to $Z\sqrt{\frac{\rho t}{A}}$. These equations were used to estimate the dE and $d\theta_{RMS}$ caused by each fiducial in order to understand the relationship between these quantities and the resulting dose perturbations. Based on the material compositions reported by the manufacturer, effective values for the atomic number Z_{eff} and atomic mass A_{eff} of each fiducial were used in these estimates. Please note that only very rough estimates of Z_{eff} and A_{eff} were used in the calculations for the PEKK polymer because its chemical composition is proprietary; however, Z_{eff} and A_{eff} are very similar for almost all plastics. The strength of any linear correlations found was quantified by calculating the correlation coefficient (r^2 value).

3. Results

3.1 Physical characteristics of fiducials

A brief description of the material composition, shape, and size of each fiducial in this study is listed in Table 1, and photographs of all the fiducials are shown in Figure 2. The fiducials

will henceforth be referred to by the fiducial names given in the first column of Table 1. Table 2 lists the mass *m*, the physical thickness *t*, and the mass thickness ρt of each fiducial.

3.2 Radiographic Visibility

Lateral and AP kV images of the fiducial markers inside the anthropomorphic phantom are shown in Figures 2 and 3, respectively. For the lateral kV images, the 40% ZrO_2 polymer rod and the 20% $BaSO_4$/PEKK polymer tube were not visible, and the long C-coated ZrO_2 3 bump rod was faint but still discernible; remainder of the fiducials were clearly visible. For the AP kV images, all of the fiducials were clearly visible except for the 20% $BaSO_4$/PEKK polymer tube, which was faint but still discernible. For the CT images of the pelvic phantom, all the fiducials were clearly visible except for the 20% $BaSO_4$/PEKK polymer tube. Although the radiographic visibility of the thick carbon-coated ZrO_2 rod on CT images was not verified, since all of the other carbon-coated ZrO_2 fiducials were clearly visible, it is a fair assumption that the thick carbon-coated ZrO_2 rod would also be visible on CT images. The results of all radiographic visibility tests are summarized in Table 1.

3.3 Quantification of Streak Artifacts

Based on a comparison of the calculated values of the streak index *SI*, the C-coated W rod and C-coated Pt rod caused the greatest streak artifacts while the long C-coated ZrO_2 3 bump rod caused the least streak artifacts (Table 1). This quantitative result agrees with a visual assessment of the CT images since the streaks caused by the C-coated W rod and C-coated Pt rod are clearly visible (Figure 4a) compared to the other fiducials which caused minimal streak artifacts (Figure 4b).

3.4 Dose Perturbation Measurements

The relative dose perturbation (ΔD) is plotted as a function of distance downstream of the fiducial for implantation depths of 22.2 cm and 25.7 cm WET (Figures 5 and 6), and the maximum dose perturbation (ΔD_{max}) caused by each fiducial at both implantation depths is listed in Table 2. In general, the dose perturbations were greater when the fiducials were placed near the end of the proton beam's range (25.7 cm) compared to the middle of the SOBP (22.2 cm), which is consistent with previous studies (Cheung *et al*., 2010; Newhauser *et al*., 2007a; Newhauser *et al*., 2007b). For fiducials located at 22.2 cm (middle of the SOBP), there was no distance downstream of the fiducials where there was a clear maximum in the magnitude of ΔD (Figure 3). At this implantation depth, the ΔD_{max} for each fiducial ranged from 4% to 18%, and all of the fiducials except the C-coated W rod and Pt fiducials had a $\%\Delta D_{max}$ of less than 10% (Table 2). For the measurements taken with the fiducials placed approximately 1 cm from the end of the proton's range (25.7 cm), dose perturbations were reported only for points downstream of the fiducial that fell confidently within the SOBP of the proton beam in order to avoid the large dose gradients at the end of the proton beam's range. The ΔD increased steadily until the end of the proton range was reached for fiducials at this implantation depth (Figure 4), and the ΔD_{max} caused by each fiducial ranged from 3% to 47%. Only the small C-coated ZrO_2 sphere, the thin C-coated ZrO_2 rod, the C-coated ZrO_2 3 bump rod, and the 20% $BaSO_4$ /PEKK polymer tube had a $\Delta D_{max} \leq 10\%$ at this implantation depth (Table 2).

In Figure 7, the ΔD_{max} caused by each fiducial at implantation depths of 22.2 cm and 25.7 cm is plotted against estimates of the decrease in energy *dE* and the change in characteristic scattering angle $d\theta_{RMS}$ of a proton as it travels through that fiducial.

4. Discussion

In order to assess the clinical utility of several prototype fiducials for proton therapy of the prostate, we evaluated each fiducial marker based on three criteria: radiographic visibility in kV portal images, CT streak artifacts, and perturbations of proton absorbed dose. In the radiographic imaging portion of this study, the 20% $BaSO_4$ /PEKK polymer tube and the 40% ZrO_2 polymer rod , both of which had low densities compared to the other fiducial markers (0.88 and 1.4 g/cm^3 respectively),were the only fiducial markers that were not visible in kV lateral portal images. This result suggests that there is a correlation between the mass density of the fiducial and its radiographic visibility in kV portal imaging, and that for a given marker size and imaging technique, there is a minimum density required for a fiducial to be clearly visible.

Various metrics have been proposed to quantify the severity of streak artifacts on CT images. Van der Schaaf *et al* (2006) quantified metal streak artifacts caused by surgical clips with the volume of artifact and the number of white radiating streaks. Leng *et al* (2008) defined the total variation (*TV*) of the CT image as a figure of merit to quantify streaking artifacts. Imai *et al* (2009) employed the largest difference between adjacent CT values for line profiles that were placed almost perpendicular to streak artifacts as an index for measuring streak artifacts. In this study, we adapted Imai's index in order to quantify the severity of radial streaks instead of parallel streaks and defined our own streak index *SI*, the largest difference between CT values in a ring-shaped region of interest surrounding a fiducial marker, normalized by the standard deviation of CT values in a homogenous region free of streak artifacts. The difference beween our index *SI* and Imai's index is that a ring-shaped ROI is used instead of a rectangular one and that our index is normalized by the standard deviation of CT number is a homogenous region near the ROI. This quantitative method of calculating *SI* agreed well with qualitative results (i.e. a visual assessment of CT images) and seems to be well-suited for this specific application, evaluating the severity of radial streak artifacts on CT images caused by fiducial markers. Furthermore, this streak index allows for easy, quantitative comparison between different fiducial markers, and opens up the possibility to more accurately assess and optimize the size, shape, and material design of fiducial markers.

When the streak artifacts caused by individual fiducials in CT images were quantified using our streak index *SI*, the C-coated W (Z=74) and Pt (Z=78) rod fiducials caused the greatest streak artifacts. These artifacts are caused by high-Z, high density metals, which results in incomplete attenuation profiles (Barrett and Keat, 2004). Because streak artifacts in CT images of the patient can interfere with target delineation and cause errors in dose and range calculations in the treatment planning system, these results suggest that high density, high-Z metals should be avoided if possible when choosing the material composition for a fiducial marker.

The dose reduction caused by each fiducial was measured using radiochromic film. Based on a clinical tolerance level of 10 % dose reduction, several fiducials markers were eliminated as potentially suitable candidates. The rationale for this 10 % clinical tolerance level for dose heterogeneity has been justified elsewhere (Newhauser *et al*., 2007a) and is based on previous studies that have shown that dose perturbations of approximately 10 % do not adversely affect clinical outcomes for prostate cancer treatment. In this study, all fiducials were oriented perpendicular to the beam direction, the orientation which represents the best case scenario in terms of the dosimetric impact of the fiducials. Fiducials oriented parallel to the proton beam will have a greater mass thickness and thus will cause greater dose shadows. Cheung *et al*. (2010) reported a 38% dose perturbation for a carbon-coated ZrO_2 fiducial in the parallel orientation compared to 18% for perpendicular orientation. For

this reason, physicians try to implant fiducials in the perpendicular orientation at our institution. Our results also showed that dose perturbations increased by as much as 30% when the fiducial was placed near the end of range as opposed to the center of modulation; this result agrees with previous studies that suggest that implantation at the periphery of the target volume should be avoided (Cheung *et al*., 2010; Giebeler *et al*., 2009; Newhauser *et al*., 2007a). Whether or not the dose reductions near the end of range are clinically relevant depends on the fiducial implantation protocol followed by each individual institution. At our institution, two fiducial markers are implanted per patient, one in the base of the prostate and one in the contra-lateral apex of the prostate. The rationale behind this choice of fiducial number and location is based on our previous work that has shown that this specific combination of fiducials rivals the use of three fiducials in terms of accuracy of prostate alignment while minimizing the effects of CT artifacts and proton dose shadowing (Kudchadker *et al*., 2009). Furthermore, lateral margins are maintained so that the large dose gradients near the end of range of the proton beam are avoided. Thus, the end of range dose perturbations are not clinically relevant for the protocol followed at our institution. However, for institutions that do implant fiducials close to the periphery of the prostate (or liver) for proton therapy, the dose heterogeneities near the end of range should be kept ≤10% as well. Based on our analysis of the dose perturbation data, a positive correlation was found between the magnitude of the dose perturbation and the mass thickness, proton linear stopping power, and proton linear scattering power of a fiducial. These results suggest that a thin fiducial with low density and low atomic number will cause smaller dose perturbations in a proton beam.

Although each of the criteria (radiographic visibility, CT streak artifacts, and dose perturbations) was evaluated separately in this study, it is important to note that these criteria are not independent of each other. Photoelectric absorption is a dominant interaction for photons in the diagnostic imaging energy range (kV), and the probability of interaction via photoelectric absorption is proportional to cube of the atomic number, i.e., Z^3. Therefore, fiducials made of higher Z materials will be more easily seen in kV diagnostic images. Furthermore, more photon attenuation will occur for fiducials with greater mass thickness (ρt). Therefore, thick, dense fiducials composed of high-Z materials will exhibit greater contrast in kV radiographs and will thus be more easily visible using this imaging modality. On the other hand, high-Z, high density materials will cause greater streak artifacts in CT images as well as greater proton dose perturbations. It is clear from the results of this study, that the best fiducial marker designs involve compromises between competing criteria; specifically, designing the optimal fiducial marker requires balancing radiographic visibility against streak artifacts and dose perturbations. Importantly, new results from this work suggest that the three performance criteria used to evaluate the fiducials can be quantified (e.g. by using the proposed streak index), and that the proton dose perturbations can be modeled with simple, semi-empirical relations that depend on the material's Z, ρ, and t. Together, for the first time, the streak index and semi-empirical dose relationships make possible the mathematical statement of a single figure of merit, i.e., an objective function suitable for use with an optimization algorithm. Future work involving Monte Carlo simulations could be used to optimize material composition, shape, and dimensions of fiducials based on this figure of merit without the need to fabricate every prototype fiducial of interest.

A major strength of this study is that we evaluated and compared twelve fiducials, including one in clinical use at our institution, with various shapes, sizes, and material compositions, based on several clinically relevant criteria. Although other studies have been done involving fiducial marker visibility in kV imaging and dose perturbations caused by markers in a proton beam, there have not been any studies involving such a variety of fiducials markers or a study in which the CT streak artifacts caused by the fiducials was assessed

quantitatively along with the radiographic visibility and dose perturbations (Lim *et al*., 2009). A limitation of this study is that the visibility of the fiducials was verified for kV X-rays and CT only, and not for other imaging modalities that can be used in IGRT, such as MRI and ultrasound. Although MV portal imaging was not a focus in this study, we did image the fiducials in the anthropomorphic phantom using this imaging modality. With the lower contrast of MV imaging, only the C-coated W and C-coated Pt fiducials were clearly visible inside the phantom. Although we agree that MV imaging is an important aspect of photon radiotherapy setup verification and that visibility in MV imaging would greatly expand the usefulness of these fiducial markers, our study is focused on the use of fiducials for proton therapy and thus, the fact that the majority of the markers were not visible in MV imaging is not an issue. Furthermore, another limitation of this study is that dose shadow measurements were taken with the fiducials in two separate batches. It would be preferable to load all the fiducials into the phantom and irradiate them at the same time, eliminating any slight variations in beam output and phantom orientation, compression, or position that might exist between the two batches. However, the physical size of the phantom prohibited loading all twelve fiducials at once; the dose measurement for a fiducial could potentially be perturbed by neighboring fiducials due to the close proximity of the fiducials in this arrangement. Thus, the fiducials were split into two batches to avoid any interactions between fiducials. An additional limitation of this study is that although the fiducials were imaged in tubes containing tissue equivalent bolus in order to closely mimic a fiducial marker implanted in a patient, it is possible that small air gaps were present in between the fiducial and the phantom. These air gaps, though small, could be a source of error in our *SI* calculations.

Based on the results of this study, carbon-coated ZrO_2 (Z_{eff} = 56) would be a judicious choice for fiducial material because this material represents a good compromise between radiographic visibility and dose perturbations; its Z_{eff} is not as high as some of the metals in this study, such as platinum or tungsten, and it will therefore not cause such severe streak artifacts or dose perturbations. Furthermore, all of the carbon-coated ZrO_2 fiducials in this study were visible in kV images. However, the 40% ZrO_2/Pebax® polymer rod was faint compared to the other fiducials in both AP and lateral kV images, suggesting that a minimum percentage of ZrO_2 needs to be present in the fiducial to ensure good radiographic visibility. (Henry *et al*., 2005) investigated the optimal length and diameter of gold cylindrical fiducial markers for radiotherapy verification using electronic portal imaging, but there has not been a study on the optimal size, shape, and mass thickness of carbon-coated ZrO_2 fiducials. In particular, the minimum mass thickness of a carbon-coated ZrO_2 required for maintaining good visibility would be of interest since thinner fiducials cause lower dose perturbations. The general recommendations that can be extracted from this study (mid-Z material, minimize mass thickness while maintaining good radiographic visibility) as well as the proposed figure of merit can be applied to the design of more exotic fiducials, such as strings of fiducial markers on a bio-absorbable strand or coiled fiducials (Fuller and Scarbrough, 2006), as well as novel applications of fiducials, such as implanting fiducial markers along with source seeds for image guidance in prostate brachytherapy followed by external beam radiation (Welsh *et al*., 2004).

5. Conclusions

In this study, twelve fiducial markers, eleven of which are prototype fiducials and one that is routinely used clinically at our institution, were evaluated to determine their suitability for use in proton therapy of prostate cancer. The best fiducial markers were radiographically visible in kV portal images, caused minimal streak artifacts in CT images, and caused minimal dose perturbations when placed in a proton beam (≤10%). Based on the results of our experiments, three of the prototype fiducials (the small C-coated ZrO_2 sphere, the thin

C-coated ZrO_2 rod, and the C-coated ZrO_2 3 bump rod) met all of these criteria and were deemed excellent candidates for application in proton therapy of the prostate. However, the requirements of a fiducial marker used for proton therapy depends on the specific application as well as the implantation protocols (i.e. the location and number of markers implanted). Thus, each institution must evaluate this data in the context of its specific needs.

Acknowledgments

The authors would like to thank Joey Cheung, B.S. and Aman Anand, Ph.D. for their generous help with the film measurements. The authors would also like to thank Carbon Medical Technologies, Inc. for supplying the prototype fiducials used in this study. This work was supported in part by the National Cancer Institute (award 1 R01 CA131463-01A1). One of the authors, Jessie Huang, would like to acknowledge financial support from the Graduate School of Biomedical Sciences, UT Health Science Center at Houston.

References

Butson MJ, Yu PKN, Cheung T, Metcalfe P. Radiochromic film for medical radiation dosimetry. Mat. Sci. Eng. R. 2003; 41:61–120.

Cheung J, Kudchadker RJ, Zhu XR, Lee AK, Newhauser WD. Dose perturbations and image artifacts caused by carbon-coated ceramic and stainless steel fiducials used in proton therapy for prostate cancer. Phys. Med. Biol. 2010; 55:7135–47. [PubMed: 21076190]

Chow JCL, Grigorov GN. Dose measurements near a non-radioactive gold seed using radiographic film. Phys. Med. Biol. 2005; 50:N227–N34. [PubMed: 16148390]

Daftari I, Castenadas C, Petti PL, Singh RP, Verhey LJ. An application of GafChromic MD-55 film for 67.5 MeV clinical proton beam dosimetry. Phys. Med. Biol. 1999; 44:2735–45. [PubMed: 10588281]

Fuller, CD.; Scarbrough, TJ. Fiducial markers in image-guided radiotherapy of the prostate. US Oncological Disease. 2006.

Giebeler A, Fontenot J, Balter P, Ciangaru G, Zhu R, Newhauser W. Dose perturbations from implanted helical gold markers in proton therapy of prostate cancer. J. Appl. Clin. Med. Phys. 2009; 10:63–70.

Henry AM, Stratford J, Davies J, McCarthy C, Swindell R, Sykes J, Moore CJ, Price P, Khoo VS. An assessment of clinically optimal gold marker length and diameter for pelvic radiotherapy verification using an amorphous silicon flat panel electronic portal imaging device. Br. J. Radiol. 2005; 78:737–41. [PubMed: 16046426]

Hsu A, Pawlicki T, Luxton G, Hara W, King CR. A study of image-guided intensity-modulated radiotherapy with fiducials for localized prostate cancer including pelvic lymph nodes. Int. J. Radiat. Oncol. Biol. Phys. 2007; 68:898–902. [PubMed: 17459610]

Kudchadker RJ, Lee AK, Yu ZH, Johnson JL, Zhang L, Zhang Y, Amos RA, Nakanishi H, Ochiai A, Dong L. Effectiveness of using fewer implanted fiducial markers for prostate target alignment. Int J Radiat Oncol Biol Phys. 2009; 74:1283–9. [PubMed: 19427750]

Kupelian P, Willoughby T, Meeks S, Forbes A, Wagner T, Maach M, Langen K. Intraprostatic fiducials for localization of the prostate gland: monitoring intermarker distances during radiation therapy to test for marker stability. Int. J. Radiat. Oncol. Biol. Phys. 2005; 63:S302–S.

Lim YK, Kwak J, Kim DW, Shin D, Yoon M, Park S, Kim JS, Ahn SH, Shin J, Lee SB, Park SY, Pyo HR, Kim DY, Cho KH. Microscopic gold particle-based fiducial markers for proton therapy of prostate cancer. Int. J. Radiat. Oncol. Biol. Phys. 2009; 74:1609–16. [PubMed: 19616746]

Nederveen AJ, Dehnad H, van der Heide UA, van Moorselaar RJA, Hofman P, Lagendijk JJW. Comparison of megavoltage position verification for prostate irradiation based on bony anatomy and implanted fiducials. Radiother. Oncol. 2003; 68:81–8. [PubMed: 12885456]

Newhauser W, Fontenot J, Koch N, Dong L, Lee A, Zheng YS, Waters L, Mohan R. Monte Carlo simulations of the dosimetric impact of radiopaque fiducial markers for proton radiotherapy of the prostate. Phys. Med. Biol. 2007a; 52:2937–52. [PubMed: 17505081]

Newhauser WD, Koch NC, Fontenot JD, Rosenthal SJ, Gombos DS, Fitzek MM, Mohan R. Dosimetric impact of tantalum markers used in the treatment of uveal melanoma with proton beam therapy. Phys. Med. Biol. 2007b; 52:3979–90. [PubMed: 17664589]

Niroomand-Rad A, Blackwell CR, Coursey BM, Gall KP, Galvin JM, McLaughlin WL, Meigooni AS, Nath R, Rodgers JE, Soares CG. Radiochromic film dosimetry: recommendations of AAPM Radiation Therapy Committee Task Group 55. Med. Phys. 1998; 25:2093–115. [PubMed: 9829234]

Piermattei A, Miceli R, Azario L, Fidanzio A, delle Canne S, De Angelis C, Onori S, Pacilio M, Petetti E, Raffaele L, Sabini MG. Radiochromic film dosimetry of a low energy proton beam. Med. Phys. 2000; 27:1655–60. [PubMed: 10947269]

Ptaszkiewicz M, Weber A, Swakon J, Klosowski M, Olko P, Bilski P, Michalec B, Czopyk L. Dose perturbation behind tantalum clips in ocular proton therapy. Radiat. Meas. 2010; 45:694–7.

Soares CG. Radiochromic film dosimetry. Radiat. Meas. 2006; 41:S100–S16.

Vatnitsky SM. Radiochromic film dosimetry for clinical proton beams. Appl. Radiat. Isotopes. 1997; 48:643–51.

Welsh JS, Berta C, Borzillary S, Sam C, Shickell D, Nobile L, Greenberg M, Weiss S, Detorie N. Fiducial markers implanted during prostate brachytherapy for guiding conformal external beam radiation therapy. Technol. Cancer Res. Treat. 2004; 3:359–64. [PubMed: 15270586]

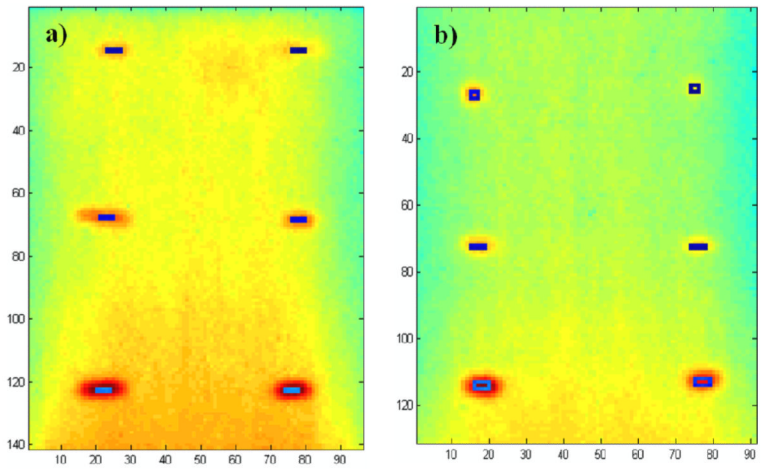

Figure 1.
Digitized images of radiochromic film (one from each batch of fiducials irradiated). Both films were irradiated near the end of proton range. Transmission values were averaged over the rectangular pixel regions shown.

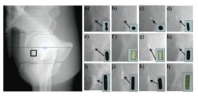

Figure 2.
kV lateral images (120 kVp, 200 mA, 630 ms) of fiducial markers inside an anthropomorphic phantom. Blown up insets of the kV images along with photographs of the fiducials themselves are shown for a) C-coated ZrO_2 barbell, b) small C-coated ZrO_2 sphere, c) large C-coated ZrO_2 sphere, d) thin C-coated ZrO_2 rod, e) thick C-coated ZrO_2 rod, f) 40% ZrO_2 polymer rod, g) 80% ZrO_2 polymer rod, h) C-coated ZrO_2 3 bump rod, i) long C-coated ZrO_2 3 bump rod, j) C-coated W rod, k) C-coated Pt rod, and l) 20% $BaSO_4$/PEKK polymer tube.

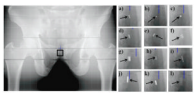

Figure 3.

AP lateral images (75 kVp, 200 mA, 80 ms) of fiducial markers inside an anthropomorphic phantom. Blown up insets are shown for a) C-coated ZrO_2 barbell, b) small C-coated ZrO_2 sphere, c) large C-coated ZrO_2 sphere, d) thin C-coated ZrO_2 rod, e) thick C-coated ZrO_2 rod, f) 40% ZrO_2 polymer rod, g) 80% ZrO_2 polymer rod, h) C-coated ZrO_2 3 bump rod, i) long C-coated ZrO_2 3 bump rod, j) C-coated W rod, k) C-coated Pt rod, and l) 20% $BaSO_4$/PEKK polymer tube.

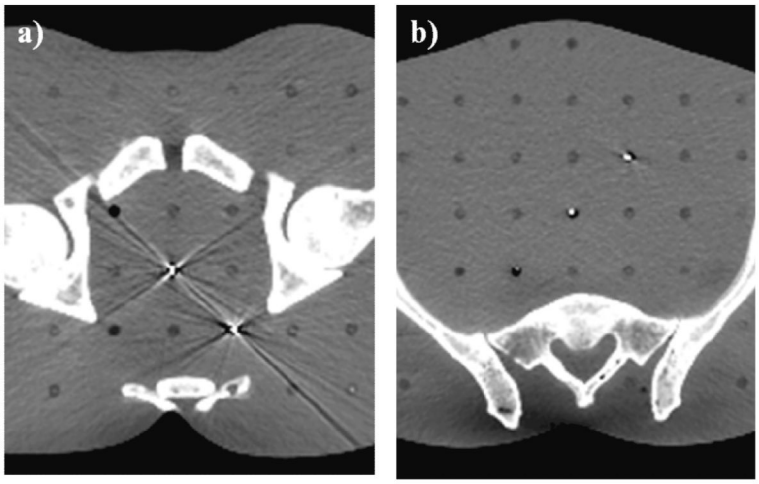

Figure 4.
CT slice image (120 kVp, 250 mAs, 2.5 mm slice thickness, 1.2695 mm pixel spacing) demonstrating (a) clearly visible streak artifacts due to the C-coated W rod (center) and carbon coated Pt (bottom right) fiducials and (b) minimal streak artifacts due to the C-coated ZrO_2 barbell (top right), the C-coated ZrO_2 3 bump rod (center), and the long C-coated ZrO_2 3 bump rod (bottom left).

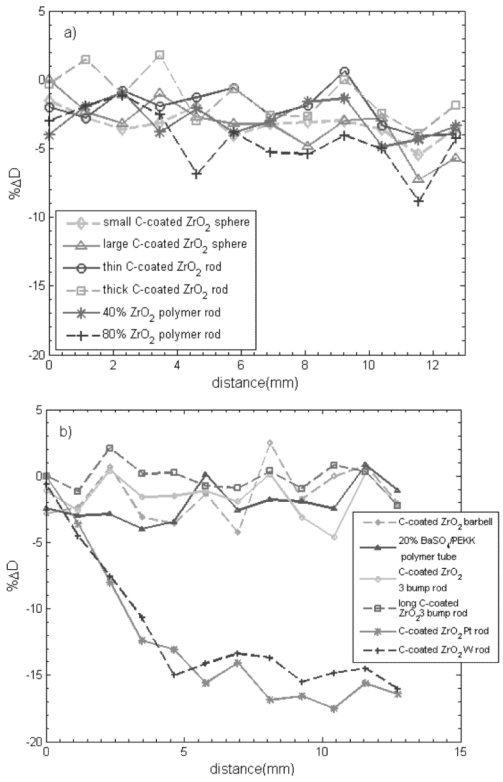

Figure 5.

Dose perturbation relative to the unperturbed dose as a function of distance downstream of the fiducial at an implantation depth of 22.2 cm WET, which corresponds to approximately the middle of the SOBP. Please note that these results are reported on two separate plots because the measurements were performed separately for two batches of fiducials (six in each batch) due to the limited size of the phantom used for dose measurements.

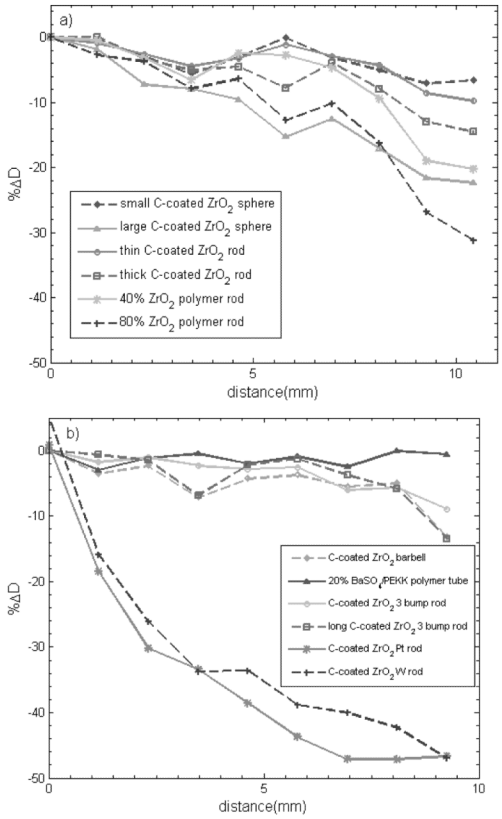

Figure 6.

Dose perturbation relative to the unperturbed dose as a function of distance downstream of the fiducial at an implantation depth of 25.7 cm WET, which corresponds to approximately 1 cm upstream of the end of range of the proton beam. Note that these results are reported on two separate plots because the measurements were performed separately for two batches of fiducials (six in each batch) due to the limited size of the phantom used for dose measurements.

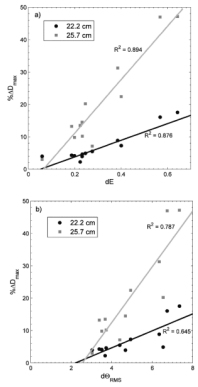

Figure 7.

The maximum percentage of dose perturbation caused by each fiducial at two depths (22.2 cm and 25.7 cm) plotted against estimates of the decrease in proton energy (a) and the change in the characteristic scattering angle (b).

Table 1

Summary of the results for the radiographic visibility and CT streak artifact quantification studies for all twelve fiducials.

Fiducial name	Description	Radiographic visibility		Streak Artifacts	
		kV lateral	kV AP	CT	SI
C-coated ZrO_2 barbell	Barbell-shaped, BiomarC® carbon-coated ZrO_2	yes	yes	yes	13.4
small C-coated ZrO_2 sphere	carbon-coated ZrO_2 sphere with 1 mm diameter	yes	yes	yes	9.1
large C-coated ZrO_2 sphere	carbon-coated ZrO_2 sphere with 1.5 mm diameter	yes	yes	yes	8.9
thin C-coated ZrO_2 rod	carbon-coated ZrO_2 rod with 0.69 mm core diameter and 0.94 total diameter	yes	yes	yes	9.1
thick C-coated ZrO_2 rod	carbon-coated ZrO_2 rod with 0.69 mm core diameter and 1.26 total diameter	yes	yes	n/a[a]	n/a[a]
40% ZrO_2 polymer rod	Cylindrical shape, composite material with 40% ZrO_2 and 60% Pebax® polymer	no	yes	yes	7.4
80% ZrO_2 polymer rod	Cylindrical shape, composite material with 80% ZrO_2 and 20% Pebax® polymer	yes	yes	yes	12.6
C-coated ZrO_2 3 bump rod	carbon-coated ZrO_2 rod with 3 bumps, 0.69 mm core diameter and 1.26 total diameter	yes	yes	yes	8.2
long C-coated ZrO_2 3 bump rod	Longer carbon-coated ZrO_2 rod with 3 bumps, 0.69 mm core diameter and 1.26 total diameter	faint	yes	yes	5.8
C-coated W rod	Carbon-coated tungsten rod	yes	yes	yes	34.0
C-coated Pt rod	Carbon-coated platinum rod, 0.69 mm core diameter and 1.26 total diameter	yes	yes	yes	42.1
20% $BaSO_4$/PEKK polymer tube	Cylindrical tube with pores, composite material with 20% $BaSO_4$ and 80% 35 poly(ether ketone ketone) (PEKK) polymer	no	faint	no	n/a[b]

[a] The thick C-coated ZrO2 rod was excluded from the CT streak artifact quantification portion of this study because it was temporarily misplaced.

[b] The 20% BaSO4/PEKK polymer tube was excluded from the CT streak artifact quantification portion of this study because it was not visible on CT images of the pelvic phantom.

Table 2

Summary of the physical characteristics of each fiducial (mass *m*, density ρ, thickness *t*, mass thickness ρt) and percent maximum dose perturbation % ΔD_{max} at two implantation depths, 22.2 cm and 25.7cm. The thickness listed is the maximum thickness along the direction of the proton beam and depends on the orientation of the fiducial during irradiation.

Fiducial name	m (mg)	ρ (g/cm^3)	t (mm)	ρt (g/cm^2)	ΔD_{max} (%)	
					22.2 cm depth	25.7 cm depth
C-coated ZrO_2 barbell	6	5.9	0.77	0.45	−4	−13
small C-coated ZrO_2 sphere	<1	1.3	1.15	0.14	−5	−7
large C-coated ZrO_2 sphere	7	3.2	1.61	0.51	−7	−22
thin C-coated ZrO_2 rod	3	1.7	0.87	0.15	−4	−10
thick C-coated ZrO_2 rod	8	2.3	1.17	0.26	−4	−15
40% ZrO_2 polymer rod	13	1.4	1.91	0.27	−5	−20
80% ZrO_2 polymer rod	20	2.6	1.79	0.46	−9	−31
C-coated ZrO_2 3 bump rod	9	2.5	1.17	0.30	−5	−10
long C-coated ZrO_2 3 bump rod	12	2.4	1.09	0.26	−2	−13
C-coated W rod	50	14.3	1.01	1.44	−16	−47
C-coated Pt rod	47	12.0	1.17	1.40	−18	−47
20% $BaSO_4$/PEKK polymer tube	5	0.88	0.62	0.05	−4	−3